

Short Excited-State Lifetimes Enable Photo-Oxidatively Stable Rubrene Derivatives

Jack Ly,[†] Kara Martin,[†] Simil Thomas,^{‡,‡,#} Masataka Yamashita,[§] Beihang Yu,[†] Craig A. Pointer,[∇] Hiroko Yamada,[§] Kenneth R. Carter,[†] Sean Parkin,^{||} Lei Zhang,^{*,†,⊥} Jean-Luc Bredas,^{*,‡,#} Elizabeth R. Young,^{*,∇} and Alejandro L. Briseno^{*,†,^}

[†]Department of Polymer Science and Engineering, University of Massachusetts, 120 Governors Drive, Amherst, Massachusetts 01003, United States

[‡]School of Chemistry and Biochemistry, Center for Organic Photonics and Electronics (COPE), Georgia Institute of Technology, Atlanta, Georgia 30332-0400, United States

[§]Graduate School of Materials Science, Nara Institute of Science and Technology (NAIST), 8916-5 Takayama-cho, Ikoma, Nara 630-0192, Japan

^{||}Department of Chemistry, University of Kentucky, Lexington, Kentucky 40506, United States

[⊥]College of Energy, Beijing Advanced Innovation Center for Soft Matter Science and Engineering, Beijing University of Chemical Technology, Beijing 100029, China

[#]Laboratory for Computational and Theoretical Chemistry of Advanced Materials, Division of Physical Science and Engineering, King Abdullah University of Science and Technology, Thuwal 23955-6900, Kingdom of Saudi Arabia

[∇]Department of Chemistry, Lehigh University, Bethlehem, Pennsylvania 18015, United States

[^]The Pennsylvania State University, Department of Chemistry, University Park, Pennsylvania 16803, United States

Supporting Information

ABSTRACT: A series of rubrene derivatives were synthesized and the influence of the side group in enhancing photo-oxidative stability was evaluated. Photo-oxidation half-lives were determined via UV–vis absorption spectroscopy, which revealed thiophene containing derivatives to be the most stable species. The electron affinity of the compounds did not correlate with stability as previously reported in literature. Our work shows that shorter excited-state lifetimes result in increased photo-oxidative stability in these rubrene derivatives. These results confirm that faster relaxation kinetics out-compete the formation of reactive oxygen species that ultimately degrade linear oligoacenes. This report highlights the importance of using molecular design to tune excited-state lifetimes in order to generate more stable oligoacenes.



INTRODUCTION

Oligoacenes with linearly annellated benzene units have received a great deal of attention in both experimental and theoretical studies because of their high-performance properties in organic electronic devices. For example, pentacene and its derivatives have proven to be one of the most successful organic semiconductors for organic thin-film transistors due to their high charge-carrier mobilities.^{1–7} As oligoacene size is varied, the electronic properties are modulated in a predictable manner. For example, as oligoacenes increase in length, their absorption red shifts, their intermolecular electronic couplings become stronger, and their larger conjugated cores result in reduced reorganization energies.^{8–12} Unfortunately increasing oligoacene size also results in deleterious changes to some properties including reduced solubility and rapid degradation, such as photo-oxidation and dimerization.^{13–15} We have previously reported the adoption of an unconventional

“angular” mode of annulation to afford more stable oligoacenes.^{16–18} This type of motif increases both the aromaticity and required distortion energy to form the oxidized *endo*-peroxide. However, one of the most common strategies to increase solubility and stability in this class of small molecules is through the addition of bulky substituents, such as phenyl, arylthio, or ethynyl moieties, at *peri*-positions.^{19–21} The enhanced stability of oligoacenes via addition of certain substituents has been attributed to the combination of steric resistance and electronic effects.^{19–22} Inclusion of bulky substituents at the *peri*-positions has proven to be a successful approach to reducing dimerization that has also served to improve solubility. However, even substituted oligoacenes still

Received: May 6, 2019

Revised: August 10, 2019

Published: August 26, 2019

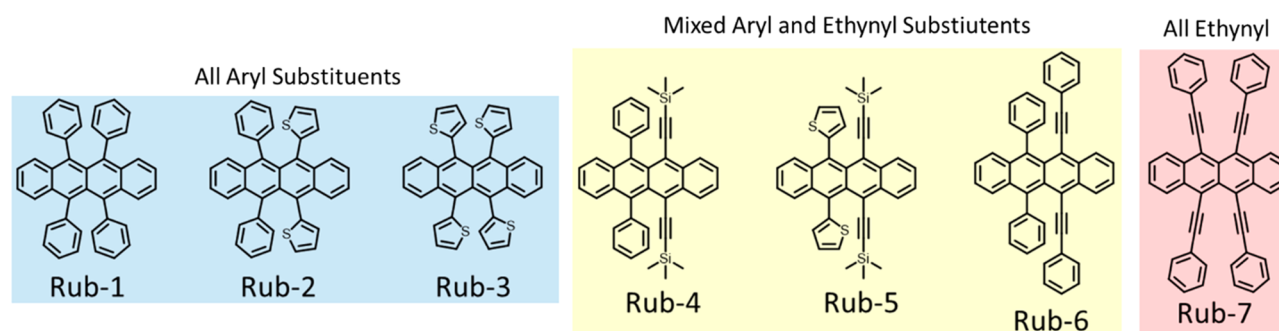


Figure 1. All-aryl, mixed aryl and ethynyl, and all-ethynyl rubrene derivatives studied in this report.

suffer from photo-oxidation in both solution and the solid state.¹⁰

Ongoing discussion and experimentation have, thus far, not been able to provide a consistent figure of merit or measurement that directly correlates oligoacene chemical structure and photostability. For example, Kaur et al. have shown that, contrary to common perception, ethynyl-type side groups are not the best-choice substituent. Silylethynyl-substituted pentacenes, TIPS-pentacenes, are in fact not the longest-lived species under photo-oxidative conditions; instead, it is the alkylthio- and arylthio-substituted pentacenes that are found to be most resistant to photo-oxidation.¹⁹ Maliakal et al. explained the increased photostability of alkynyl-pentacenes by their low-lying LUMO energy relative to pentacene.²⁰ However, Linker and co-workers have determined that fast competitive physical quenching of $^1\text{O}_2$ by ethynyl-substituted pentacenes is also key to their persistence.²³

Tetracene is another model compound with high reactivity to oxygen that can be used to investigate chemical stability. Several derivatives of substituted tetracenes have been reported, including diethynyltetracenes, tetraalkyltetracenes, dialkoxytetracenes, and rubrene derivatives.^{22,24–26} Notably, rubrene has been extensively studied for many years because of its extremely high carrier mobility.^{27–34} Indeed, it is well-known that rubrene undergoes a fast oxidation process if exposed to air. This oxidation process is strongly enhanced in the presence of light and may be thermally reversed to form the parent compound.³⁵ It has also been reported that, among rubrene derivatives (tetrasubstituted tetracenes), the side groups that result in lowering LUMO levels and imparting steric hindrance of the acene core display stability improvement over the benchmark rubrene molecule.²⁴ However, thiophene-containing derivatives have also shown significant resistance toward photo-oxidation, which does not follow this rationale.²⁵ Due to the fact that few rubrene derivatives have been reported, the effect of the substituents on the photo-oxidation has not been fully comprehended, leaving a gap in understanding about their oxidation process and what can be done to mitigate rubrene degradation.

To address this issue, a library of six rubrene derivatives was synthesized and investigated for photo-oxidative stability for comparison against commercially available benchmark rubrene (**Rub-1**) via a facile solution-state photo-oxidation experiment. Here, the synergistic photostabilization effects of aryl, ethynyl, and combinations of those and other side groups for rubrene derivatives are explored. To our surprise, we did not observe a correlation between deeper electron affinities, commonly referred to as the LUMO energies, and increased stability of the rubrene derivatives.³⁶ We therefore extended our

characterization of the rubrene derivatives to include their photophysical properties. Excited-state dynamics experiments of rubrene derivatives were determined via time-resolved photoluminescence and transient absorption spectroscopy. This report reveals that oligoacenes with shorter excited-state lifetimes, rather than larger electron affinities, result in long-lived and more photo-oxidatively stable compounds. We postulate that more rapid excited-state decay kinetically outcompetes the photosensitization and generation of reactive oxygen species, thus enabling longer-lived species. We found that thiophene analogues produced the shorter-lived rubrene excited states and ultimately more stable rubrene derivatives.

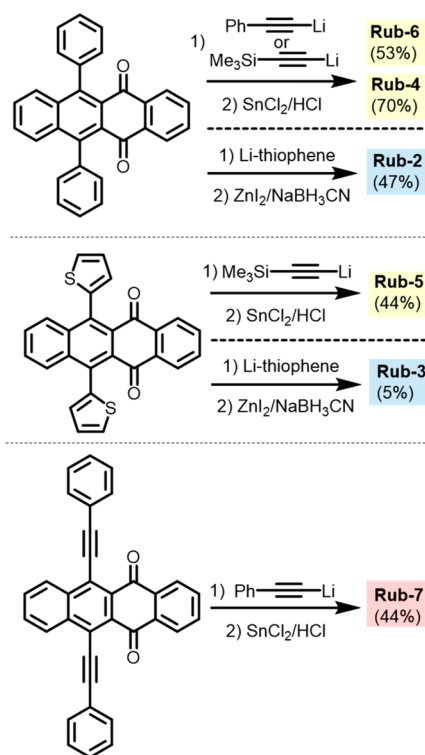
RESULTS AND DISCUSSION

Synthesis, Molecular Characterization, and Electronic Structure. The rubrene derivatives studied in this report are shown in **Figure 1**. Here, rubrene side groups are modified with varying combination of phenyl, thiophenyl, trimethylsilyl ethynyl, and phenyl ethynyl groups. The synthetic pathway to these analogues was carried out in a two-step process: previously reported quinones were added to a THF solution of lithiated substituents followed by a reductive aromatization step with either SnCl_2 or ZnI_2 for the addition of ethynyl and thiophene motifs, respectively (**Scheme 1**).^{37,38} Synthetic protocols and characterization are reported in the Supporting Information (**Figure S1–S11**). Target molecules were obtained in moderate yields apart from **Rub-3**, which was isolated in very low yields.

Figure 2A shows the absorption spectra of rubrene derivatives obtained via UV–vis spectroscopy. Derivatives containing only aryl-substituents (**Rub-1**, **Rub-2**, and **Rub-3**) exhibit the most blue-shifted absorption spectra. Compared to the **Rub-1** peak absorption at 531 nm, the **Rub-2** and **Rub-3** spectra are slightly red-shifted by 3 nm (0.01 eV) and 7 nm (0.03 eV), respectively. This small redshift in absorption is a result of the increased electron donating inductive effect of thiophene as compared to phenyl substitution. This is supported by a deeper shift in the ionization potential (IP) and electron affinity (EA) displayed in **Figure 2B**.

The mixed aryl- and ethynyl-substituted rubrene derivatives produce a cluster of closely grouped absorption spectra that are red-shifted compared to the all-aryl substituted rubrene derivatives. The red-shifted spectra observed for this group occurs as a result of the extended conjugation of the rubrene core afforded by the ethynyl groups. A modest redshift of 2 nm in peak absorption is observed in **Rub-5** compared to **Rub-4**, again due to stronger inductive effect of thiophene. Among the mixed aryl and ethynyl derivatives, **Rub-6** exhibits the most red-shifted peak absorption at 578 nm, an 11 nm redshift

Scheme 1. Two-Step Synthesis Pathway from Known Quinones to Afford Rubrene Derivatives



compared to **Rub-4**. This redshift was attributed to extended conjugation of phenyl acetylene substituent compared to the ethynyl $\text{Si}(\text{Me})_3$. Overall, increasing ethynyl content resulted in longer absorption wavelengths. This effect is most dramatically observed in **Rub-7** with the most red-shifted peak absorption at 638 nm as it contains exclusively phenyl acetylene substituents.

Cyclic voltammetry (CV) was performed in dichloromethane with 0.1 M tetrabutylammonium hexafluorophosphate as the supporting electrolyte to measure the oxidation and reduction onsets used to calculate the ionization potentials (IP) and electron affinity (EA) energies of the derivatives

(Figure 2B and Figure S12). Overall, there is a disproportionate shift in the EA among the target molecules compared to the relatively unperturbed IP. This result suggests that the HOMO of these molecules is stabilized by the tetracene core and does not depend on the substituents added to the moiety. In agreement with results observed in the UV-vis spectra, thieryl substituents reveal a modest effect, lowering the electrochemical bandgap (E_g) in **Rub-2** and **Rub-3** only slightly as compared to **Rub-1** by 0.05 and 0.11 eV, respectively. Ethynyl substitutions yielded the most profound effect upon the bandgap with **Rub-7** having the deepest EA energy of -3.6 eV. Based upon literature precedent, materials with the lowest lying EA energy would be predicted to be the most stable material, meaning that **Rub-7** would be the most stable of the prepared compounds in this study.^{20,21}

Kinetics of Photo-Oxidation. To rank the substitution effect upon photo-oxidative stability, chloroform solutions of each rubrene derivative (2.0×10^{-5} M) were prepared and exposed to ambient light and air at room temperature. UV-vis measurements were taken at various times to track the photo-oxidation process (Figure 3A). An example of this experiment is shown in Figure 3B for benchmark **Rub-1**. After affirming the spectral shape did not change, normalized peak wavelength absorption-time profiles for each of the rubrene derivatives were plotted, Figure 3C and 3D. These rubrene derivatives were subjected to identical conditions so that the measured half-lives could be directly compared.¹⁹ Normalized peak absorbance-time profiles were plotted for each derivative to yield the relative stability toward photo-oxidation as follows: (most stable) **Rub-3** > **Rub-2** > **Rub-5** > **Rub-7** > **Rub-6** > **Rub-4** > and **Rub-1** (least stable). The observed stability does not correlate with the molar absorption coefficients of the rubrene derivatives. Negligible degradation was observed over a 24 h period in the dark.

To our surprise, a negligible increase in photo-oxidative stability was observed in **Rub-4** and **Rub-6** as compared to the commercially available **Rub-1**. Previous reports consistently remark that acetylene-type substituents enhance stability of pentacene compared to 6,13-bisphenyl pentacene analogues via lowering of the LUMO, and thus lower triplet energy to retard the sensitization of reactive oxygen-species.^{15,20} Others have postulated that the bis-ethynyl functionality enables the

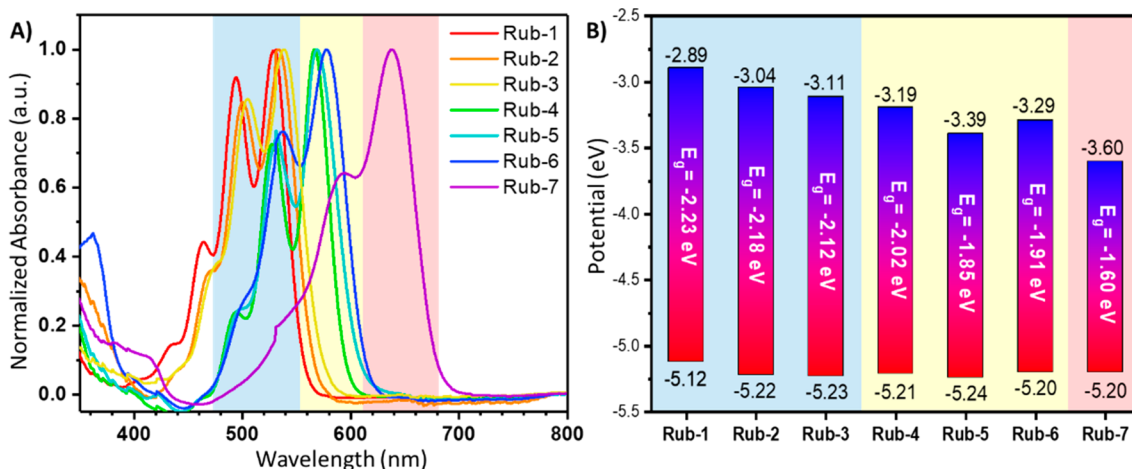


Figure 2. (A) UV-vis spectra of rubrene derivatives in chloroform and (B) energy level diagram of the derivatives determined from cyclic voltammetry. The IPs and EAs were determined by solution state CV in CH_2Cl_2 . The potentials were determined with ferrocene (Fc) as standard by the formula: $\text{IP} = -(E_{\text{onset}}^{\text{ox}} - E_{\text{Fc}/\text{Fc}^+}^{1/2} + 4.8)$ eV and $\text{EA} = -(E_{\text{onset}}^{\text{red}} - E_{\text{Fc}/\text{Fc}^+}^{1/2} + 4.8)$ eV, wherein $E_{\text{Fc}/\text{Fc}^+}^{1/2} = 0.53$ eV.

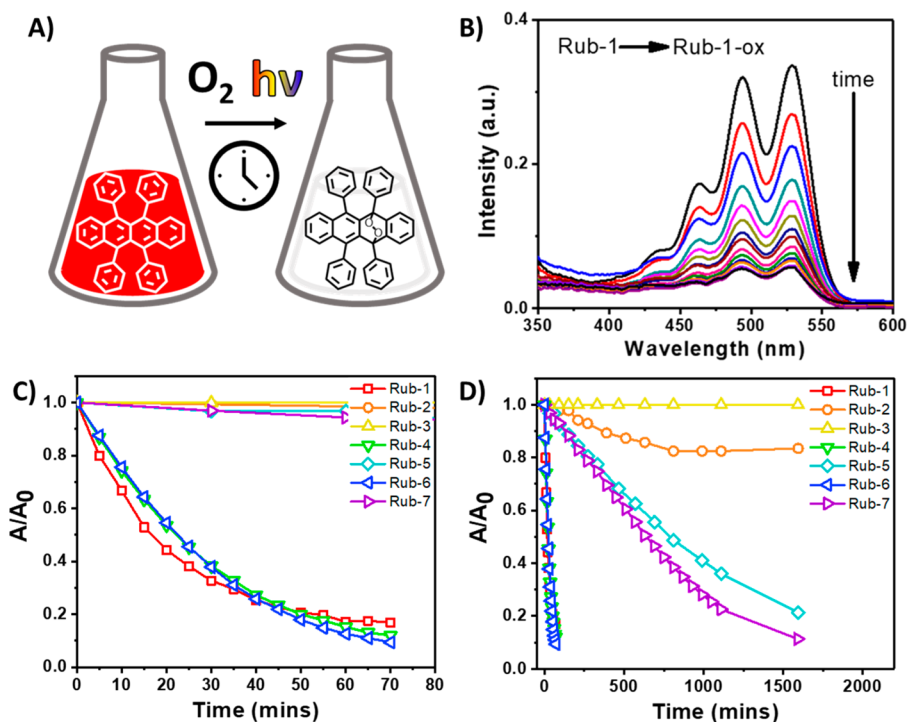


Figure 3. (A) Photo-oxidation of 2.5×10^{-5} M rubrene solution in CHCl_3 under ambient conditions, (B) absorption degradation profile spectra of Rub-1, and (C and D) normalized peak absorption-time profiles of rubrene analogues in short and extended time ranges, respectively.

physical quenching of $^1\text{O}_2$ ²³ for increased stability, however, this effect is negligible and/or nonoperative in these studies as **Rub-6** rapidly degrades on the same order as **Rub-1**. Tetracene has a shorter conjugation length than that of pentacene, thus the bandgap is appreciably larger, and this mechanism is no longer relevant to consider as revealed by transient absorption spectroscopy (vide infra). A noticeable decrease of the EA energy was observed with **Rub-7**, which did result in an order of magnitude increase in observed half-life compared to **Rub-1**. This result is consistent with the notion that lower LUMO levels increase the oxidative stability of oligoacenes, however, **Rub-7** was not the most stable rubrene derivative, as would have been expected based solely on the EA stabilization metric.

Thiophene containing species (**Rub-2**, **Rub-3**, and **Rub-5**) showed the greatest resistance to photo-oxidation. The optical and electronic properties, summarized in Table 1, did not show significant correlation with the stability among these materials. Thieryl- and ethynyl-containing **Rub-5** has very similar characteristics to **Rub-4** and **Rub-6** yet **Rub-5** is nearly 40 times more stable. An even more drastic comparison is noted

between the strictly aryl-containing species; phenyl and thienyl containing **Rub-2** is at least three orders more stable than **Rub-1** while no degradation of **Rub-3** is observed. These results are reminiscent of work by Kaur et al. that report alkylthio- and arylthio-substituted pentacenes were far more stable than the ethynyl analogue.¹⁹ Thus, the narrative of electronic contribution of choice side groups must be challenged and reconsidered from these experimental results; they do not have an apparent trend upon photo-oxidative stability of tetra-substituted tetracenes.

Molecular Structures and Crystal Geometries. To understand how molecular design affects steric hindrance and its impact on upon photo-oxidative stability, backbone torsion caused by the peri-positioned side groups are examined. Solution-borne materials were analyzed via single crystal X-ray crystallography. Individual molecules are shown in Figure 4. The degrees of backbone twist were defined via the terminal sp^2 carbons C_1 and C_2 orientation to C_3 and C_4 .

Table 1. Optical, Electrochemical, and Half-Life Properties of Rubrene Derivatives

compound	optical		electrochemical			half-life (mins)
	λ_{max} (nm)	E_g (eV)	IP (eV)	EA (eV)	E_g (eV)	
Rub-1	531	2.19	-5.12	-2.89	2.23	17
Rub-2	534	2.15	-5.22	-3.04	2.18	>2400
Rub-3	538	2.08	-5.23	-3.11	2.12	very stable
Rub-4	567	2.04	-5.21	-3.19	2.02	22
Rub-5	569	2.02	-5.24	-3.39	1.85	795
Rub-6	578	1.98	-5.20	-3.29	1.91	22.5
Rub-7	638	1.79	-5.20	-3.60	1.60	635

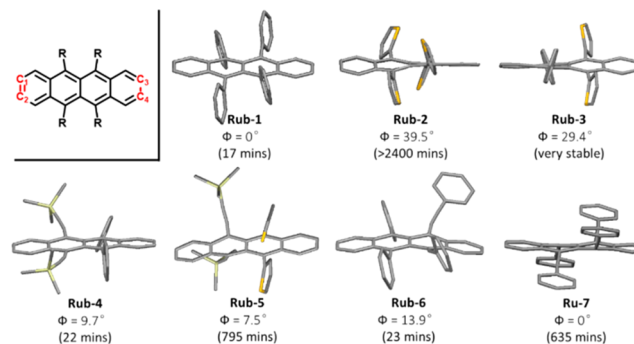
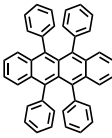
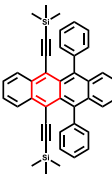
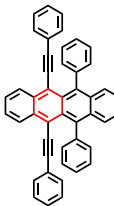
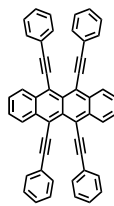
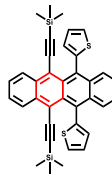
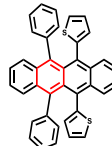
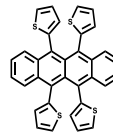


Figure 4. Torsion angle along the backbone (Φ) was determined by the C-C double bonds at either end of the tetracene backbone (labeled as C_1 , C_2 , C_3 , and C_4). Lifetimes are shown in parentheses.

Table 2. Measured Half-Life Values and Calculated Transition State Energies (ΔG^\ddagger) for All Rubrene Analogues^a

	Rub-1	Rub-4	Rub-6	Rub-7	Rub-5	Rub-2	Rub-3
Half-life (mins)	17	22	22.5	635	795	>2400	Very Stable
ΔG^\ddagger (kcal/mol)	23.8	23.7 (26.3)	22.7 (26.1)	24.8	25.0 (26.2)	26.2 (26.3)	27.6
							

^aEnergies were calculated at the DLPNO-CCSD(T)+M06-2X/cc-pVTZ//M06-2X/cc-pVDZ level of theory. Highlighted energies reflect the preferred endoperoxide formation.

Although compounds **Rub-1** and **Rub-7** showed planar conformation of the tetracenes, **Rub-2** and **Rub-3** have twisted core conformations. It is likely that the interactions between the side substituents strongly contribute to the planarization of the tetracene cores. All the phenyl and thienyl substituents rotated away from a coplanar conformation with the tetracene backbone and lead to less conjugation, affirming the reduced electronic effect these groups have on the tetracene core as previously mentioned. **Rub-2** and **Rub-3** with at least two thienyl substituents have larger twisted tetracene cores with torsions of 29.4° and 39.5°, respectively. The backbone twist along the tetracene core is a consequence of interplay between the intramolecular exchange-repulsion interaction of select side groups and intermolecular interactions in the solid state as previously described.³⁹

Formed endoperoxides from the photo-oxidation of **Rub-1**, **Rub-4**, **Rub-5**, and **Rub-6** were purified and isolated in high yields. Single crystal analysis showed formation of the endoperoxide were stereoselective across the acetylene functionalized ring, where applicable (see Supporting Information, Figure S13). It is presumed the steric congestion by the adjacent aryl group drives the stereoselectivity toward the acetylene functionalized rings. Endo-peroxide forms of **Rub-2**, **Rub-3**, and **Rub-7** were not detected due to low yield, suggesting these species may undergo other degradation pathways in CHCl₃ or the endo-peroxide form was not stable either.

Quantum-Chemical Calculations. In the spirit of our earlier study on the oxidation stability of bistetracenes, we carried out quantum-chemical calculations to examine how the transition-state free energies (ΔG^\ddagger), calculated on the basis of the oligoacene ground-state electronic structure, compare to the photo-oxidation kinetics, Table 2. The computational details are given in section 9 of the SI.^{40,41} The results demonstrate that in all derivatives the preferred oxidation pathway involves a concerted rather than stepwise mechanism (see SI, Figures S18–S24 and Table S2). The calculated transition-state free energies (ΔG^\ddagger) are actually found to correlate with the measured half-life values.

In the case of derivatives where the central rings of the backbone are substituted by different groups, the transition-state energies were evaluated on both inner rings to gauge the

regioselectivity of endoperoxide formation. A lower ΔG^\ddagger energy is calculated for endoperoxide formation across the ethynyl substituted rings in **Rub-4**, **Rub-5**, and **Rub-6**; the reaction free energies also point to the same products as thermodynamically favored, which corroborates with experimental stereoselectivity determination of endo-peroxide formation. For **Rub-2**, endo-peroxide formation was competitive on both inner rings.

Mechanism and Time Resolved Spectroscopy. While the quantum-chemical calculations correlate well with the observed photo-oxidation half-lives, there remains a need to experimentally rationalize the photo-oxidative stability in this series of rubrene analogues, especially in light of the fact that the measured IP and EA energies do not correlate with the photo-oxidative stability order. A conclusive result thus far is that thiophene moieties cause the system to be more resistant to photo-oxidation. In order to shed more light onto this matter, it is thus useful to investigate more deeply the photophysical properties of these derivatives.

The mechanism to endo-peroxide formation, the likely degradation pathway for the series of rubrene moieties, results from interaction between the oligoacene and reactive oxygen species. The sensitization of O₂^{•-} and ¹O₂ may occur through either type 1 or type 2 photo-oxidation, shown in Scheme 2. First, light is absorbed to promote the acene to an excited singlet state. Excitation is followed by two possible processes: (1) relaxation of the excited state, either through radiative (fluorescence) or nonradiative decay to the ground state, or (2) intersystem crossing of the singlet state to the triplet state

Scheme 2. Photo-Mechanism of endo-Peroxide Formation

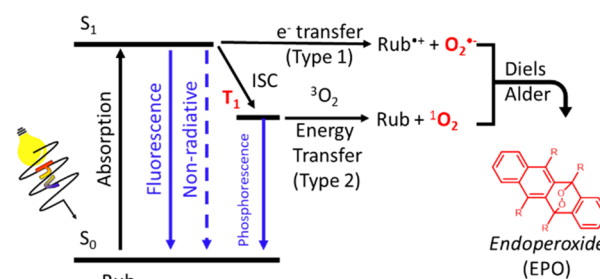


Table 3. Rubrene Derivatives Arranged in the Order of Photo-Oxidation Half-Life Tabulated against Fluorescence Quantum Yield (Φ_F), Emission Lifetimes (τ_F), Radiative (τ_r), and Non-Radiative (τ_{nr}) Lifetimes Determined from Time-Resolved Photoluminescence (trPL)

	half-life	quantum yield	emission lifetimes	radiative lifetime	nonradiative lifetime
	$\tau_{1/2}$ (min)	Φ_F (%)	τ_F (ns)	τ_r (ns)	τ_{nr} (ns)
Rub-1	17	84 (100) ⁴¹	14.37 \pm 0.25	17.11	89.9
Rub-4	22	~100	15.93 \pm 0.21	16.09	N/A
Rub-6	22.5	~100	10.75 \pm 0.07	10.85	N/A
Rub-7	635	8.37	0.86 \pm 0.01	10.27	0.93
Rub-5	795	2	0.44 \pm 0.09 ^a	22.00	0.44
Rub-2	>2400	0.24	0.12 \pm 0.01	50.00	0.12
Rub-3	(stable)	N/A	0.32 \pm 0.04		

^aA second component of 2.91 ns with contribution of <8% was obtained in the fit and corresponds to anomalous scattering from the excitation pulse. **Rub-3** showed negligible fluorescence intensity that was not reliable for determining Φ_F , which is therefore reported as N/A. With no Φ_F for **Rub-3**, τ_r and τ_{nr} could not be determined.

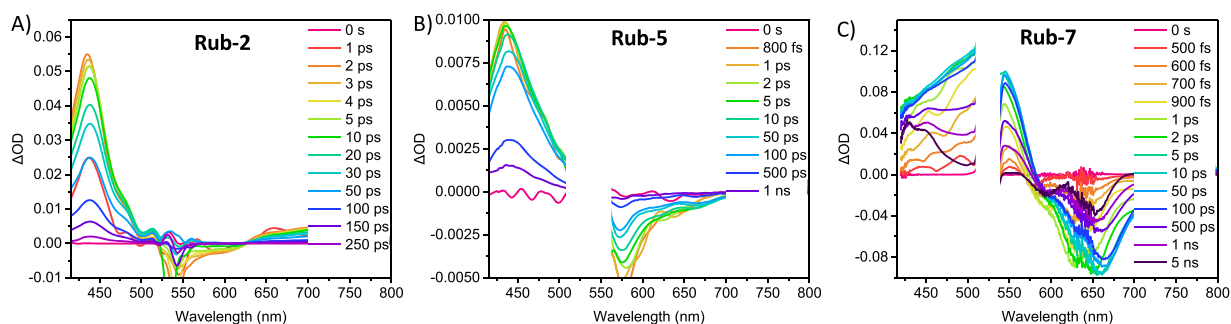


Figure 5. fs-transient absorption spectra for very stable (A) **Rub-2**, intermediately stable (B) **Rub-5**, and (C) **Rub-7**. Singlet kinetic decay profiles were obtained by fitting the single wavelength trace at 510 nm for **Rub-1**, 434 nm for **Rub-2**, 438 nm for **Rub-3**, 485 nm for **Rub-4**, 435 nm for **Rub-5**, 480 nm for **Rub-6**, and 544 nm for **Rub-7**. **Rub-2**, **Rub-5**, and **Rub-7** were excited at 560 nm and show similar broad absorption bands associated with the singlet excited state of rubrene, concomitant with a ground state bleach. **Rub-7** shows the evolution of a triplet state.

which can decay through phosphorescence or nonradiatively. However, in the presence of oxygen, electron or energy transfer can also occur from the (1) singlet or (2) triplet state of the acene to the triplet ground state of oxygen to produce $O_2^{\bullet-}$ and 1O_2 , respectively. These $O_2^{\bullet-}$ and 1O_2 species are very reactive and have been implicated as a primary culprit in photobleaching of organic compounds. As photo-oxidative degradation is an excited-state phenomenon, understanding the photophysical characteristics of the tetrasubstituted tetracenes is crucial to understanding why certain derivatives show higher oxidative stability.

Femtosecond and nanosecond transient absorption (TA) and time-resolved photoluminescence (trPL) were conducted to observe excited-state decay rates of radiative and non-radiative pathways for all rubrene derivatives. The mirror image nature of the spectral shape of the absorbance (Figure 2A) and fluorescence spectra (Figure S14) suggest that absorption and emission occur from the singlet state. TrPL is used to measure the singlet excited-state emission decay lifetimes across all rubrene derivatives, while TA gives radiative and nonradiative singlet excited-state decay lifetimes for all rubrene derivatives, as well as insight into the photophysical processes involved in the excited-state deactivation in **Rub-7** (Table 4).

Time-correlated single photon counting (TCSPC) was used to collect transient emission profiles of each sample (Figure S16). The entire emission peak of each rubrene sample was integrated and used to produce a single kinetic trace, with good reproducibility and signal-to-noise ratios. The samples for trPL were prepared in the glovebox with dry chloroform. For **Rub-4**,

Rub-6, **Rub-7**, **Rub-2**, and **Rub-3**, a single emission lifetime was extracted by fitting a monoexponential function to the emission decay profile, while for **Rub-5**, two lifetimes were extracted from a biexponential fit of the emission decay profile, one of which is attributed to anomalous scattering into the detector. The emission lifetimes obtained through trPL are tabulated in Table 3. Using the experimentally determined emission quantum yields (Figure S15 and Table S1) and these emission lifetimes, both the radiative and nonradiative lifetimes were calculated using the relation, $k_r = \frac{\Phi_F}{\tau_F}$, $k_{nr} = \frac{(1-\Phi_F)}{\tau_F}$, and $\tau_r = \frac{1}{k_r}$ (or $\tau_{nr} = \frac{1}{k_{nr}}$) and are reported in Table 3. Among synthetically obtained molecules, **Rub-6** and **Rub-4** reveal two of the longer emission lifetime decays (τ_F) at ~11 and ~15 ns, respectively and the highest fluorescence quantum yields. The near unity quantum yield means that a nonradiative lifetime cannot be calculated. **Rub-1**, which also shows long emission lifetimes and high quantum yields produced the larger calculated nonradiative lifetime (~90 ns). When considering the photophysical data, a trend emerges, namely rubrene derivatives with shorter nonradiative lifetimes (i.e., smaller τ_{nr} values) show the largest $t_{1/2}$ values. Indeed, **Rub-3** ($\tau_F = 0.35$ ns) and **Rub-2** ($\tau_F = 0.13$ ns) possess the shortest emission lifetimes and low or essentially undetectable quantum yields, meaning that their τ_{nr} values are the smallest of the synthesized moieties. **Rub-3** and **Rub-2** as well as derivatives with longer half-lives have quantifiable fluorescent lifetimes, however, they also have considerably low quantum yields, indicating the

Table 4. Lifetimes Obtained by Single Wavelength Fitting of TA Data Compared to the Oxidative Half-Life^a

	$\tau_{1/2}$ (min)	τ_1 (ps)	A ₁	τ_2 (ps)	A ₂	τ_3 (ps)	A ₃	Triplet (μ s)
Rub-1	17	14100 ± 2580 ^r						
Rub-4	22	16600 ± 3670 ^r						
Rub-6	22.5	12400 ± 1740 ^r						
Rub-7	635	871 ± 20.6 ^r	82.5%	412 ± 10.2	17.5%			25.5 ± 1.50
Rub-5	795	455 ± 21.7 ^r	87%	22.6 ± 8.52	13%			
Rub-2	>2400	48.2 ± 0.150	73.1%	125 ± 5.30 ^r	26.9%			
Rub-3	(stable)	24.7 ± 1.60	89.3%	53.2 ± 4.60	8.1%	211 ± 4.6 ^r	2.6%	

^aThe lifetimes in light yellow are assigned to radiative lifetimes by comparison to trPL (Table 3), while the lifetimes in blue are assigned to non-radiative decay pathways. Lifetimes were obtained by fitting the single wavelength trace at 510 nm for **Rub-1**, 434 nm for **Rub-2**, 438 nm for **Rub-3**, 490 nm for **Rub-4**, 435 nm for **Rub-5**, 480 nm for **Rub-6**, and 544 nm for **Rub-7**. Triplet lifetime for **Rub-7** was obtained by fitting the single wavelength trace at 460 nm in ns-TA.

primary mode of singlet decay occurs through rapid non-radiative pathways.

Both femtosecond (fs-TA) and nanosecond (ns-TA) transient absorption experiments were performed to characterize the nature of the excited-state evolution for each rubrene moiety. Samples were prepared in an inert glovebox environment using dry chloroform. No photodegradation of the rubrene derivatives occurred during TA measurements as UV-vis measurements taken before and after laser exposure were identical. Rubrene derivatives were excited at 470 or 560 nm depending on the location of absorption band of the respective rubrene moiety. The excited-state evolution of **Rub-1**, **Rub-2**, **Rub-3**, **Rub-4**, **Rub-5**, and **Rub-6** were recorded with fs-TA (Figure 5 and Figure S16). **Rub-7** excited-state evolution revealed longer lifetimes and was recorded with both fs-TA and ns-TA (Figure S16). The fs-TA of each rubrene moiety shows a ground-state bleach that matches the absorption profile of each moiety. Excited-state absorption associated with the singlet excited state is seen to the blue of each ground-state bleach. For several rubrene moieties (**Rub-1**, **Rub-2**, **Rub-3**, and **Rub-6**) an additional, less intense, excited-state absorption is observed to the red of the ground-state bleach. The fs-TA spectra of **Rub-1**, **Rub-2**, **Rub-3**, **Rub-4**, and **Rub-5** essentially decay back to the ground state with little shift in the excited-state absorption bands. In these moieties, the bleach recovery and excited-state decay occur with similar kinetics meaning that the primary decay pathway occurs via radiative or nonradiative decay from the singlet excited state back to the ground state. The single wavelength decay (at approximately the 440 nm peak) is fitted to either bi- or triexponential functions. The lifetimes for each rubrene species are reported in Table 4.

For each rubrene species radiative lifetimes can be identified by comparing the lifetimes to the radiative and nonradiative lifetimes determined through trPL and quantum yield measurements (Table 3) to the lifetimes obtained through single-wavelength fitting. Those lifetimes that correspond to the radiative lifetime found from trPL are indicated by an r superscript and labeled with yellow boxes in Table 4. The additional lifetimes correspond to the nonradiative decay pathways from this singlet state (labeled with blue boxes). The most oxidatively stable rubrene species (**Rub-3** and **Rub-2**)

reveal, not only the shortest overall lifetimes, but also that the largest contribution to their excited-state decay originates from nonradiative pathways that generally possess smaller τ_{nr} values, rather than the radiative pathway. For example, **Rub-3**, one of the most photo-oxidatively stable rubrenes presented in this study, shows a dominant nonradiative decay lifetime of ~ 25 ps that accounts for $\sim 89\%$ of the decay profile, with minimal ($<3\%$) contribution from the radiative pathways. Additionally, **Rub-2** reveals a dominant nonradiative (~ 50 ps) decay pathway accounting for $>70\%$ of fitted signal. The intermediately stable rubrene complexes (**Rub-5** and **Rub-7**), on the other hand, show substantial contribution from the radiative pathway ($\sim 87\%$ and $\sim 83\%$) with some contribution from a nonradiative process. The least photo-oxidatively stable complexes (**Rub-6**, **Rub-4**, and **Rub-1**), however, reveal no contribution from nonradiative decay.

Rub-7 was analyzed using both fs-TA and ns-TA. This derivative showed a broad singlet absorption band at ~ 540 nm that decayed concurrent with initial ground-state bleach recovery. The singlet, however, in this moiety was able to undergo intersystem crossing to form a triplet state that grew in at 460 nm in fs-TA. The triplet state decay was observed over several microseconds using ns-TA, decaying back to the baseline within the 100 μ s window used for fitting, indicating that the long-lived species was not due to photodegradation of the **Rub-7**.

Several points regarding the mechanism for degradation can be elucidated from these photophysical studies. Because triplet formation is observed in only one rubrene moiety (**Rub-7**) the degradation mechanism involving singlet oxygen formation through type 2 energy transfer can be discounted. Therefore, if reactive oxygen species are involved in the degradation of the rubrene moieties, it likely occurs via formation of $O_2^{\bullet-}$ by electron transfer and subsequent attack of the rubrene (vide supra). Further, ultrafast lifetimes of <50 ps completely outcompete the collisional diffusion between the excited-state rubrene and molecular oxygen to form $O_2^{\bullet-}$, thus leading to little to no yield of the *endo*-peroxide. This observed relationship between photo-oxidatively resistant species and average excited-state lifetimes of the rubrene derivatives is illustrated in Figure 6, which depicts photo-oxidative half-lives versus the average singlet state lifetimes, $\langle\tau\rangle$.

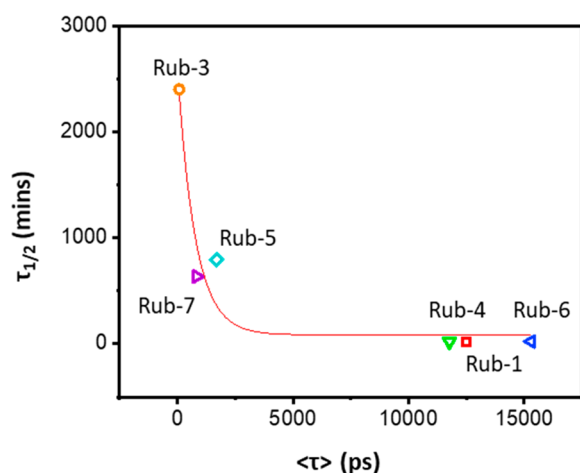


Figure 6. Determined half-life ($\tau_{1/2}$) plotted against average excited/singlet state lifetime ($\langle\tau\rangle$) of rubrene derivatives. Average lifetime is calculated by the equation: $\langle\tau\rangle = (\sum f_n \tau_n^2) / (\sum f_n \tau_n)$.⁴²

A clear trend emerges when considering the photophysics of the rubrene moieties presented in this work, namely, the lifetimes of the dominant decay pathways for the seven derivatives correlate inversely with the oxidative degradation half-lives. The excited states of the more stable derivatives decay through faster, nonradiative mechanisms, with nonstable derivatives decaying through slower, radiative mechanisms.

CONCLUSION

A library of rubrene derivatives are ranked in terms of photo-oxidative stability to study the stabilization effect of aryl, ethynyl, and combinations thereof side groups. Surprisingly, stability does not correlate with electron affinity energies as previously reported for substituted oligoacenes. The transition-state energies for *endo*-peroxide formation (ΔG^\ddagger), calculated on the basis of the oligoacene ground-state electronic structure of all derivatives, follow the experimental trends. Using transient absorption and time-resolved photoluminescence, we are able to show that increased stability is in fact directly correlated with short-lived excited states that decay primarily through nonradiative pathways. Thiophene containing molecules (**Rub-2**, **Rub-3**, and **Rub-5**) displayed the shortest-lived excited states where all-aryl type thiophene-containing analogues impart the dominant nonradiative decay to the ground state. This ultrafast decay back to the ground state kinetically out competes electron transfer, thus immensely suppressing the $O_2^{\bullet-}$ formation that ultimately photo-oxidizes the chromophore. This report highlights the importance of the photophysical kinetics for the realization and rational design of stable linear oligoacenes. The implications of this correlation between short (nonradiative) excited-state lifetimes and enhanced oxidative photostability reveal a critical design principle that can be used to generate more stable, further extended oligoacenes for high-mobility performance in organic field-effect transistors and photovoltaics.

ASSOCIATED CONTENT

Supporting Information

The Supporting Information is available free of charge on the ACS Publications website at DOI: 10.1021/acs.jpca.9b04203.

NMR, cyclic voltammetry, fluorescence, transient absorption, fluorescence quantum yield, and computational details (PDF)

Crystallographic file for **Rub-6-Ox** (CIF)

Crystallographic file for **Rub-5-Ox** (CIF)

Crystallographic file for **Rub-4** (CIF)

Crystallographic file for **Rub-7** (CIF)

Crystallographic file for **Rub-4-Ox** (CIF)

Crystallographic file for **Rub-3** (CIF)

Crystallographic file for **Rub-5** (CIF)

Crystallographic file for **Rub-6** (CIF)

Crystallographic file for **Rub-2** (CIF)

AUTHOR INFORMATION

Corresponding Authors

*E-mail: zhl@mail.buct.edu.cn.

*E-mail: jean-luc.bredas@chemistry.gatech.edu.

*E-mail: ery317@lehigh.edu.

*E-mail: alb818@psu.edu.

ORCID

Hiroko Yamada: 0000-0002-2138-5902

Kenneth R. Carter: 0000-0002-7081-2296

Lei Zhang: 0000-0002-0162-7222

Jean-Luc Bredas: 0000-0001-7278-4471

Elizabeth R. Young: 0000-0002-6509-9289

Alejandro L. Briseno: 0000-0003-2981-9143

Author Contributions

The manuscript was written through contributions of all authors. All authors have given approval to the final version of the manuscript.

Notes

The authors declare no competing financial interest.

ACKNOWLEDGMENTS

A.L.B. acknowledges the Office of Naval Research (Award N00014-16-1-2612) and the National Science Foundation (DMR-1508627). The work at Georgia Tech was supported by the Office of Naval Research (Award N00014-17-1-2208). E.R.Y. thanks the NSF Major Research Instrumentation program for funds that established the multiuser laser facility for transient absorption (CHE-1428633). K.R.C. thanks the National Science Foundation (DMR-1506968) for support. S.P. thanks the NSF MRI program for awards CHE-0319176 and CHE-1625732.

REFERENCES

- (1) Nelson, S. F.; Lin, Y.-Y.; Gundlach, D. J.; Jackson, T. N. Temperature-independent transport in high-mobility pentacene transistors. *Appl. Phys. Lett.* **1998**, *72*, 1854–1856.
- (2) Anthony, J. E.; Brooks, J. S.; Eaton, D. L.; Parkin, S. R. Functionalized pentacene: improved electronic properties from control of solid-state order. *J. Am. Chem. Soc.* **2001**, *123*, 9482–9483.
- (3) Afzali, A.; Dimitrakopoulos, C. D.; Breen, T. L. High-performance, solution-processed organic thin film transistors from a novel pentacene precursor. *J. Am. Chem. Soc.* **2002**, *124*, 8812–8813.
- (4) Klauk, H.; Halik, M.; Zschieschang, U.; Schmid, G.; Radlik, W.; Weber, W. High-mobility polymer gate dielectric pentacene thin film transistors. *J. Appl. Phys.* **2002**, *92*, 5259–5263.
- (5) Afzali, A.; Dimitrakopoulos, C. D.; Graham, T. O. photosensitive pentacene precursor: synthesis, photothermal patterning, and application in thin-film transistors. *Adv. Mater.* **2003**, *15*, 2066–2069.
- (6) Sakamoto, Y.; Suzuki, T.; Kobayashi, M.; Gao, Y.; Fukai, Y.; Inoue, Y.; Sato, F.; Tokito, S. Perfluoropentacene: high-performance

- p–n junctions and complementary circuits with pentacene. *J. Am. Chem. Soc.* **2004**, *126*, 8138–8140.
- (7) Park, S. K.; Jackson, T. N.; Anthony, J. E.; Mourey, D. A. High mobility solution processed 6,13-bis(triisopropyl-silylethynyl) pentacene organic thin film transistors. *Appl. Phys. Lett.* **2007**, *91*, 063514.
- (8) Gruhn, N. E.; da Silva Filho, D. A.; Bill, T. G.; Malagoli, M.; Coropceanu, V.; Kahn, A.; Brédas, J.-L. the vibrational reorganization energy in pentacene: molecular influences on charge transport. *J. Am. Chem. Soc.* **2002**, *124*, 7918–7919.
- (9) Brédas, J.-L.; Beljonne, D.; Coropceanu, V.; Cornil, J. Charge-transfer and energy-transfer processes in π -conjugated oligomers and polymers: a molecular picture. *Chem. Rev.* **2004**, *104*, 4971–5004.
- (10) Anthony, J. E. Functionalized acenes and heteroacenes for organic electronics. *Chem. Rev.* **2006**, *106*, 5028–5048.
- (11) Miao, Q.; Chi, X.; Xiao, S.; Zeis, R.; Lefenfeld, M.; Siegrist, T.; Steigerwald, M. L.; Nuckolls, C. organization of acenes with a cruciform assembly motif. *J. Am. Chem. Soc.* **2006**, *128*, 1340–1345.
- (12) Zhang, L.; Cao, Y.; Colella, N. S.; Liang, Y.; Brédas, J.-L.; Houk, K. N.; Briseno, A. L. Unconventional, chemically stable, and soluble two-dimensional angular polycyclic aromatic hydrocarbons: from molecular design to device applications. *Acc. Chem. Res.* **2015**, *48*, 500–509.
- (13) Reichwagen, J.; Hopf, H.; Del Guerso, A.; Desvergne, J.-P.; Bouas-Laurent, H. Photodimers of a soluble tetracene derivative. excimer fluorescence from the head-to-head isomer. *Org. Lett.* **2004**, *6*, 1899–1902.
- (14) Zade, S. S.; Zamoshchik, N.; Reddy, A. R.; Fridman-Marueli, G.; Sheberla, D.; Bendikov, M. Products and mechanism of acene dimerization. a computational study. *J. Am. Chem. Soc.* **2011**, *133*, 10803–10816.
- (15) Zade, S. S.; Bendikov, M. Reactivity of acenes: mechanisms and dependence on acene length. *J. Phys. Org. Chem.* **2012**, *25*, 452–461.
- (16) Cao, Y.; Liang, Y.; Zhang, L.; Osuna, S.; Hoyt, A.-L. M.; Briseno, A. L.; Houk, K. N. Why bistetracenes are much less reactive than pentacenes in diels–alder reactions with fullerenes. *J. Am. Chem. Soc.* **2014**, *136*, 10743–10751.
- (17) Thomas, S.; Ly, J.; Zhang, L.; Briseno, A. L.; Brédas, J.-L. Improving the stability of organic semiconductors: distortion energy versus aromaticity in substituted bistetracene. *Chem. Mater.* **2016**, *28*, 8504–8512.
- (18) Zhang, L.; Fonari, A.; Liu, Y.; Hoyt, A.-L. M.; Lee, H.; Granger, D.; Parkin, S.; Russell, T. P.; Anthony, J. E.; Brédas, J.-L.; Coropceanu, V.; Briseno, A. L. Bistetracene: An air-stable, high-mobility organic semiconductor with extended conjugation. *J. Am. Chem. Soc.* **2014**, *136*, 9248–9251.
- (19) Kaur, I.; Jia, W.; Kopreski, R. P.; Selvarasah, S.; Dokmeci, M. R.; Pramanik, C.; McGruer, N. E.; Miller, G. P. Substituent Effects in Pentacenes: gaining control over homo–lumo gaps and photo-oxidative resistances. *J. Am. Chem. Soc.* **2008**, *130*, 16274–16286.
- (20) Maliakal, A.; Raghavachari, K.; Katz, H.; Chandross, E.; Siegrist, T. Photochemical stability of pentacene and a substituted pentacene in solution and in thin films. *Chem. Mater.* **2004**, *16*, 4980–4986.
- (21) Fudickar, W.; Linker, T. reversible photooxygenation of alkynylanthracenes: chemical generation of singlet oxygen under very mild conditions. *Chem. - Eur. J.* **2011**, *17*, 13661–13664.
- (22) Baral, R. N.; Thomas, S. W. Steric and electronic substituent effects influencing regioselectivity of tetracene endoperoxidation. *J. Org. Chem.* **2015**, *80*, 11086–11091.
- (23) Fudickar, W.; Linker, T. Why triple bonds protect acenes from oxidation and decomposition. *J. Am. Chem. Soc.* **2012**, *134*, 15071–15082.
- (24) Zhang, J.; Sarrafpour, S.; Haas, T. E.; Müller, P.; Thomas, S. W. Structure, photophysics, and photooxidation of crowded diethynyltetracenes. *J. Mater. Chem.* **2012**, *22*, 6182–6189.
- (25) Zhang, X.; Sørensen, J. K.; Fu, X.; Zhen, Y.; Zhao, G.; Jiang, L.; Dong, H.; Liu, J.; Shuai, Z.; Geng, H.; Bjørnholm, T.; Hu, W. Rubrene analogues with the aggregation-induced emission enhancement behaviour. *J. Mater. Chem. C* **2014**, *2*, 884–890.
- (26) Zhang, J.; Smith, Z. C.; Thomas, S. W. Electronic Effects of Ring Fusion and Alkyne Substitution on Acene Properties and Reactivity. *J. Org. Chem.* **2014**, *79*, 10081–10093.
- (27) Podzorov, V.; Menard, E.; Borissov, A.; Kiryukhin, V.; Rogers, J. A.; Gershenson, M. E. Intrinsic charge transport on the surface of organic semiconductors. *Phys. Rev. Lett.* **2004**, *93*, 086602.
- (28) de Boer, R. W. I.; Gershenson, M. E.; Morpurgo, A. F.; Podzorov, V. Organic single-crystal field-effect transistors. *Phys. Status Solidi A* **2004**, *201*, 1302–1331.
- (29) Podzorov, V.; Sysoev, S. E.; Loginova, E.; Pudalov, V. M.; Gershenson, M. E. Single-crystal organic field effect transistors with the hole mobility ~ 8 cm²/V s. *Appl. Phys. Lett.* **2003**, *83*, 3504–3506.
- (30) Podzorov, V.; Pudalov, V. M.; Gershenson, M. E. Field-effect transistors on rubrene single crystals with parylene gate insulator. *Appl. Phys. Lett.* **2003**, *82*, 1739–1741.
- (31) Takeya, J.; Yamagishi, M.; Tominari, Y.; Hirahara, R.; Nakazawa, Y.; Nishikawa, T.; Kawase, T.; Shimoda, T.; Ogawa, S. Very high-mobility organic single-crystal transistors with in-crystal conduction channels. *Appl. Phys. Lett.* **2007**, *90*, 102120.
- (32) Sundar, V. C.; Zaumseil, J.; Podzorov, V.; Menard, E.; Willett, R. L.; Someya, T.; Gershenson, M. E.; Rogers, J. A. Elastomeric transistor stamps: reversible probing of charge transport in organic crystals. *Science* **2004**, *303*, 1644–1646.
- (33) Bisri, S. Z.; Takenobu, T.; Takahashi, T.; Iwasa, Y. Electron transport in rubrene single-crystal transistors. *Appl. Phys. Lett.* **2010**, *96*, 183304.
- (34) da Silva Filho, D. A.; Kim, E.-G.; Brédas, J.-L. Transport properties in the rubrene crystal: electronic coupling and vibrational reorganization energy. *Adv. Mater.* **2005**, *17*, 1072–1076.
- (35) Ly, J. T.; Lopez, S. A.; Lin, J. B.; Kim, J. J.; Lee, H.; Burnett, E. K.; Zhang, L.; Aspuru-Guzik, A.; Houk, K. N.; Briseno, A. L. Oxidation of rubrene, and implications for device stability. *J. Mater. Chem. C* **2018**, *6*, 3757–3761.
- (36) Brédas, J.-L. Mind the gap! *Mater. Horiz.* **2014**, *1*, 17–19.
- (37) Paraskar, A. S.; Reddy, A. R.; Patra, A.; Wijsboom, Y. H.; Gidron, O.; Shimon, L. J. W.; Leitius, G.; Bendikov, M. Rubrenes: planar and twisted. *Chem. - Eur. J.* **2008**, *14*, 10639–10647.
- (38) Zhang, X.; Meng, Q.; He, Y.; Wang, C.; Dong, H.; Hu, W. A new pseudo rubrene analogue with excellent film forming ability, *Sci. China: Chem.* **2011**, *54*, 631–635.
- (39) Sutton, C.; Marshall, M. S.; Sherrill, C. D.; Risko, C.; Brédas, J.-L. Rubrene: the interplay between intramolecular and intermolecular interactions determines the planarization of its tetracene core in the solid state. *J. Am. Chem. Soc.* **2015**, *137*, 8775–8782.
- (40) Neese, F. The ORCA program system. *Wiley Interdiscip. Rev. Comput. Mol. Sci.* **2012**, *2*, 73–78.
- (41) Strickler, S. J.; Berg, R. A. Relationship between absorption intensity and fluorescence lifetime of molecules. *J. Chem. Phys.* **1962**, *37*, 814–822.
- (42) Christians, J. A.; Kamat, P. V. Trap and transfer. two-step hole injection across the Sb₂S₃/CuSCN interface in solid-state solar cells. *ACS Nano* **2013**, *7*, 7967–7974.